



HAL
open science

Pyrolysis of waste polyethylene in a semi-batch reactor to produce liquid fuel: optimization of operating conditions

Ruming Pan, Márcio F. Martins, Gerald Debenest

► To cite this version:

Ruming Pan, Márcio F. Martins, Gerald Debenest. Pyrolysis of waste polyethylene in a semi-batch reactor to produce liquid fuel: optimization of operating conditions. *Energy Conversion and Management*, 2021, 237, pp.114114. 10.1016/j.enconman.2021.114114 . hal-03382557

HAL Id: hal-03382557

<https://hal.science/hal-03382557>

Submitted on 18 Oct 2021

HAL is a multi-disciplinary open access archive for the deposit and dissemination of scientific research documents, whether they are published or not. The documents may come from teaching and research institutions in France or abroad, or from public or private research centers.

L'archive ouverte pluridisciplinaire **HAL**, est destinée au dépôt et à la diffusion de documents scientifiques de niveau recherche, publiés ou non, émanant des établissements d'enseignement et de recherche français ou étrangers, des laboratoires publics ou privés.



Open Archive Toulouse Archive Ouverte



OATAO is an open access repository that collects the work of Toulouse researchers and makes it freely available over the web where possible

This is an author's version published in: <https://oatao.univ-toulouse.fr/28056>

Official URL:

<https://doi.org/10.1016/j.enconman.2021.114114>

To cite this version:

Pan, Ruming  and Martins, Márcio F. and Debenest, Gérald  *Pyrolysis of waste polyethylene in a semi-batch reactor to produce liquid fuel : optimization of operating conditions.* (2021) *Energy Conversion and Management* (237). 114114. ISSN 0196-8904.

Any correspondence concerning this service should be sent to the repository administrator: tech-oatao@listes-diff.inp-toulouse.fr

Pyrolysis of waste polyethylene in a semi-batch reactor to produce liquid fuel: Optimization of operating conditions

Ruming Pan^a, Marcio Ferreira Martins^b, Gérald Debenest^{a,*}

^a Institut de Mécanique des Fluides de Toulouse (IMFT) - Université de Toulouse, CNRS-INPT-UPS, Toulouse 31400, France

^b Laboratory of Combustion and Combustible Matter (LCC), PPGEM, Federal University of Espírito Santo, Vitória 29075-910, Brazil

A B S T R A C T

Keywords:

Waste polyethylene
Thermal pyrolysis
Liquid fuel production
Optimization
Operating conditions

This study investigated the interactive effects of temperature, residence time, and carrier gas flow rate on the liquid fuel production through the pyrolysis of waste polyethylene (WPE) in a bench-scale semi-batch reactor. To enhance the liquid fuel production, fifteen experiments were conducted based on a central composite design. The adaptive neural fuzzy model was adopted to establish the relationship between liquid fuel production and operating conditions. The R-squared value of the experimental and adaptive neural fuzzy model predicted that liquid fuel production was 0.9934. Four additional experimental results verified the adaptive neural fuzzy model's applicability. Subsequently, the genetic algorithm (GA) was adopted to optimize operating conditions to maximize liquid fuel production. The GA optimized operating conditions (temperature, residence time, and carrier gas flow rate) were: 488 °C, 20 min, and 20 mL/min. The liquid fuel under the optimal operating conditions was analyzed by Fourier-transform infrared spectroscopy (FTIR) and gas chromatography-mass spectrometry (GC-MS). The liquid fuel had similar main functional groups as diesel. The components of the liquid fuel were mainly 1-alkenes and n-alkanes ranging from C7 to C36. The effects of operating conditions on liquid fuel fractions and mean molecular weight were also investigated.

1. Introduction

Municipal solid waste (MSW) is accumulating rapidly due to the enormous resource consumption and inefficient recycling worldwide. It is estimated that within 34 years (from 2016 to 2050), MSW will increase from 2.01 billion tons to 3.40 billion tons [1]. Plastic waste accounts for a large part of Municipal Solid Waste (MSW) due to its wide range of uses [2]. Moreover, the waste polyethylene (WPE) accounts for 40% of plastics in MSW [3]. Also, about 70% of the total produced plastics have been directly discarded in the environment [4]. These combinations of mismanagement have aggravated environmental pollution and endangered human health [5]. Therefore, the recycling of waste plastics, especially the WPE, needs to be further promoted.

It is reported that pyrolysis is an efficient way to recycle the WPE [6,7]. The polymer is thermally decomposed into gas, liquid fuel, and char products in an oxygen-free atmosphere. Moreover, slow pyrolysis with low heating rates can enhance liquid fuel production [8]. The thermal lag phenomenon can also be diminished by adopting low heating rates [9]. The uniform temperature distributions inside the reactor and the reactants can be achieved during slow pyrolysis [10,11].

This is conducive to heat and mass transfer and liquid fuel production [8,12]. The distribution of products is determined by the reactor type, the presence of catalysts, and operating conditions, such as temperature, residence time, and carrier gas flow rate [6]. Many studies on the thermal pyrolysis of polyethylene (PE) have been conducted in semi-batch reactors. It has been reported that high liquid fuel yields can be obtained [13–18].

In terms of operating conditions, the temperature is the dominant parameter during plastics' pyrolysis [6]. Onwudili et al. [3,19] reported that the virgin low-density PE was completely pyrolyzed at temperatures above 425 °C. The liquid fuel yield reached 89.5 wt% at 425 °C. They also found that liquid oil production dropped drastically as the temperature increased beyond 425 °C. Tiikma et al. [20] stated that the optimal temperature for the liquid oil production from the pyrolysis of the WPE was 450 °C. Quesada et al. [21,22] and Rodríguez-Luna et al. [23] investigated WPE and high-density PE thermal pyrolysis processes in a temperature range of 450–550 °C, respectively. They both reported that the optimal temperature for liquid fuel production was 500 °C. Sharuddin et al. [6] also concluded that temperatures below 500 °C were suitable for plastics' pyrolysis to produce liquid fuel.

* Corresponding author.

E-mail address: gerald.debenest@toulouse-inp.fr (G. Debenest).

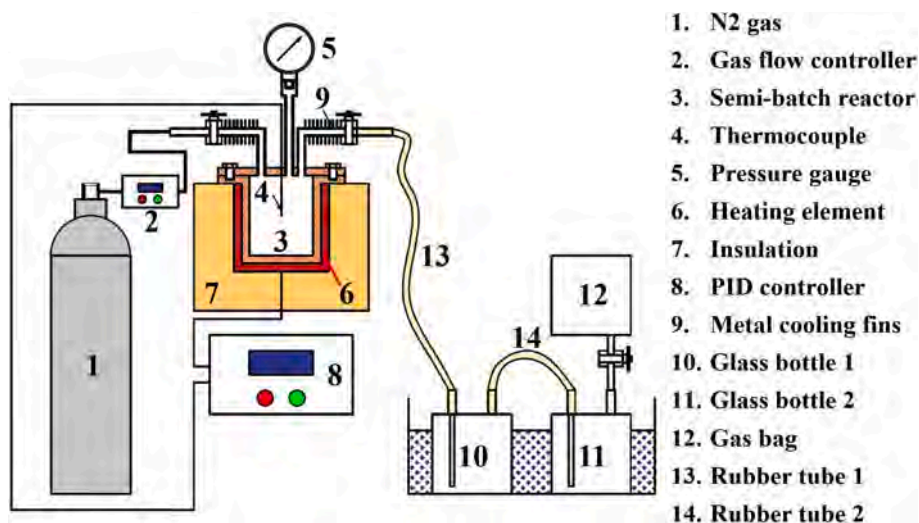


Fig. 1. The experimental schematic diagram of the pyrolysis of WPE for liquid fuel production.

According to [3], the residence time was related to the experiment's duration at the target temperature. It has been reported that the residence time is also a critical factor in determining the composition of pyrolysis products [3,21]. Quesada et al. [21,22] found that a long residence time could enhance the liquid fuel yield. Muhammad et al. [24] investigated the effect of the carrier gas flow rate on PE's pyrolysis in a 200 mL bench-scale semi-batch reactor with nitrogen as the carrier gas. They investigated the production changes of liquid fuel and char with gas flow rates in the range of 0–60 mL/min. Also, they found that the carrier gas flow rate could also determine the distribution of thermal pyrolysis products of PE. A higher carrier gas flow rate would increase the liquid fuel yield and reduce the char yield.

In short, on the one hand, many research works have been done to investigate the effects of the operating conditions (temperature, residence time, and carrier gas flow rate) on the liquid fuel yield through the pyrolysis of PE; On the other, most of them investigated such effects by varying operating conditions one-by-one. However, according to [21], the operating conditions have complex interactive effects on liquid fuel production, which requires establishing a multiparameter mathematical expression for evaluating the yield of liquid fuel. For these reasons, one-by-one relationship interaction makes the optimal operating conditions determined in such a way not particularly convincing.

The adaptive neural fuzzy model [25,26] is a suitable mathematical method that can set up relations between attributive variables and multiple arguments. Paramasivam [27] adopted the adaptive neural fuzzy model to analyze the CI engine performance through engine load and fuel mixture ratio. High accuracy was obtained between the experimental, and the adaptive neural fuzzy model predicted results. Pan et al. [28] established the mathematical relationship between the PE pyrolysis rate and the operating conditions (temperature and heating rate). The high R-squared value (>0.999) between the experimental and predicted values exhibited the adaptive neural fuzzy model's reliability. Dubdub et al. [29] utilized the adaptive neural fuzzy model to conduct the thermogravimetric modeling of high-density PE catalytic pyrolysis. A good agreement between the experimental and predicted data was also obtained. Quesada et al. [21] adopted different mathematical models to establish the relationships between the yields of plastic waste pyrolysis products and operating conditions. They concluded that the adaptive neural fuzzy model predicted results were more accurate and reliable.

In this perspective, this study aims to comprehensively investigate the interactive effects of temperature, residence time, and carrier gas flow rate on the liquid fuel production through the slow pyrolysis (heating rate of 6 °C/min) [30] of the WPE in a bench-scale semi-batch

reactor. The adaptive neural fuzzy model [25,26] was adopted to determine the liquid oil production by the operating conditions (temperature, residence time, and carrier gas flow rate). The genetic algorithm (GA) is a promising method to determine the extremums of complicated functions [7,31]. Due to the complex expressions established by the adaptive neural fuzzy model, GA was exploited to ascertain the maximum liquid fuel production's operating conditions. The adaptive neural fuzzy model was also used to investigate the effects of operating conditions on the gas yield through thermal pyrolysis of WPE. The pyrolysis liquid fuel under the optimal operating conditions was analyzed by Fourier-transform infrared spectroscopy (FTIR) and gas chromatography-mass spectrometry (GC-MS). Lastly, the effects of operating conditions on liquid fuel fractions and mean molecular weight were also investigated.

2. Material and methods

2.1. Material

WPE was provided from Wanbei Plastic Recycling Development Base in Anhui Province, China. It was recycled from MSW and cut into approximately 3 mm pellets.

2.2. Experimental setup

Fig. 1 illustrates the experimental schematic diagram of the pyrolysis of WPE for liquid fuel production. The reactor is a 200 mL bench-scale semi-batch reactor. The WPE weighing approximately 5 g was used in each experiment. The reactor was purged with nitrogen at a 100 mL/min flow rate for 30 min before each experiment to ensure an inert atmosphere, and then nitrogen flow was adjusted to the target flow rate. The internal pressure of the reactor was maintained at 0.1 MPa during the whole experiment. The reactor was heated from room temperature (20 °C) to the target temperature at a heating rate of 6 °C/min [30] in each experiment. Subsequently, the reactor was maintained at the target temperature for the specified duration (the residence time).

WPE was pyrolyzed into volatilized gas (liquid fuel and gas). The volatilized gas was purged out of the reactor by the carrier gas through the outlet pipe. The outer wall of the outlet pipe is equipped with metal cooling fins. The volatilized gas can be cooled to about 50 °C through the outlet pipe. Part of volatilized gas was condensed into liquid fuel during this process. The liquid fuel flowed through the rubber tube [24] into the glass bottle. The rest volatilized gas was condensed into a liquid by the ice-water mixture (0 °C) [23,24,32] and collected by two in-sequence

Table 1
Experiments performed under different operating conditions.

Number	Temperature (°C)	Residence time (min)	Carrier gas flow rate (mL/min)
E1	425	20	20
E2	425	20	100
E3	425	40	60
E4	425	60	20
E5	425	60	100
E6	475	20	60
E7	475	40	20
E8	475	40	60
E9	475	40	100
E10	475	60	60
E11	525	20	20
E12	525	20	100
E13	525	40	60
E14	525	60	20
E15	525	60	100
V1	450	30	80
V2	450	50	40
V3	500	30	80
V4	500	50	40

glass bottles. It is worth mentioning that liquid fuel was entirely collected in the first glass bottle. There was no liquid fuel collected in the second glass bottle. The WPE pyrolysis gas product was collected in the gas bag. Lastly, the reactor was taken out of the heating device and promptly cooled by water. The remaining contents in the reactor were char and involatile remnants [24,33,34]. The reactor was opened when it was cooled to 20 °C. The residue was then collected and weighed.

The semi-batch reactor and the glass bottle (1) and the two glass bottles are connected by the rubber tubes. The liquid fuel also excites inside the metal outlet pipe and the rubber tubes. To reduce the experimental errors, two glass bottles and two rubber tubes are all weighted. The substance inside the metal outlet pipe is also collected and weighted. The weight of liquid fuel is calculated by the following equation,

$$W_{liquid} = (W_{b1,f} + W_{b2,f} + W_{r1,f} + W_{r2,f}) (W_{b1,i} + W_{b2,i} + W_{r1,i} + W_{r2,i}) + W_{op} \quad (1)$$

where W_{liquid} , $W_{b1,f}$, $W_{b2,f}$, $W_{r1,f}$, $W_{r2,f}$, $W_{b1,i}$, $W_{b2,i}$, $W_{r1,i}$, $W_{r2,i}$ and W_{op} represent the weight of liquid fuel, the final weight of glass bottle (1), the final weight of glass bottle (2), the final weight of rubber tube (1), the final weight of rubber tube (2), the initial weight of glass bottle (1), the initial weight of glass bottle (2), the initial weight of rubber tube (1), the initial weight of rubber tube (2) and the substance weight inside the metal outline pipe, respectively.

The weight of gas is calculated by the following equation,

$$W_{gas} = W_{WPE} - W_{liquid} - W_{residue} \quad (2)$$

where W_{gas} , W_{WPE} , and $W_{residue}$ represent the weights of gas, initial WPE and residue, respectively.

A central composite design [21,35] was used to determine the optimal operating conditions of liquid fuel production. A total number of fifteen experiments were conducted to obtain the experimental results [21]. Furthermore, a mathematical expression with independent variables (temperature, residence time, and carrier gas flow rate) was established by the adaptive neural fuzzy model to investigate the production of liquid fuel. The experiments were conducted under different operating conditions, as tabulated in Table 1. Fifteen experiments were numbered from E1 to E15. Four additional experiments were conducted to validate the mathematical model established by the adaptive neural fuzzy model. Four validation experiments were numbered from V1 to V4. Each experiment was conducted two times to ensure repeatability.

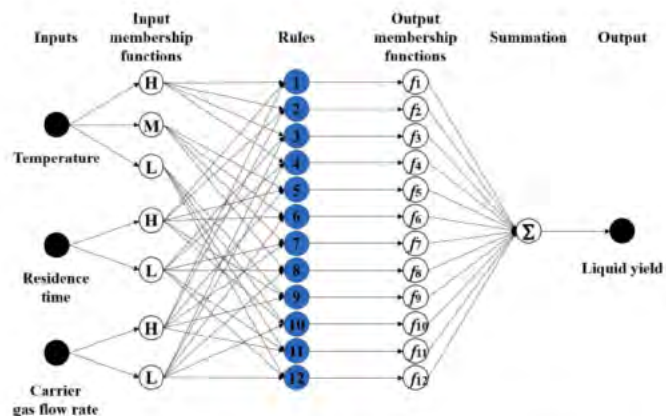


Fig. 2. The network structure of the adaptive neural fuzzy model for determining liquid fuel production.

2.3. Methods

2.3.1. The adaptive neural fuzzy model

Fig. 2 depicts the network structure of the adaptive neural fuzzy model for determining liquid fuel production. The adaptive neural fuzzy model utilizes the subsistent input and output data to determine the network structure's parameters [25,28]. The network structure connections are established by the IF-THEN fuzzy rules [26]. In this study, the network structure has three input variables (temperature, residence time, and carrier gas flow rate) and two output variables (liquid fuel and gas yields). According to [21], the temperature was divided into three levels (high, medium, and low); the residence time was divided into two levels (high and low); the carrier gas flow rate was divided into two levels (high and low). The input membership functions were combined into twelve fuzzy rules, which were determined by the Gaussian dependency function [28]. The output membership functions of constant type were served as the defuzzification functions. The weighted values of the fuzzy rules were calculated by the input and output membership functions. Lastly, the summation of the weighted values of twelve fuzzy rules was the liquid fuel production value. The adaptive neural fuzzy model is described in detail by [21,25,26,28].

2.3.2. Genetic algorithm (GA)

Genetic algorithm (GA) is a widespread optimization method [36]. GA is derived from the theory of evolution [7]. GA's core contents are the mutation and the crossover of individuals' genes, and survival of the fittest in each generation. In this study, operating conditions (temperature, residence time, and carrier gas flow rate) were three "genes". Liquid fuel fraction is the fitness of each individual. GA, coupled with the adaptive neural fuzzy model, was utilized to optimize the operating conditions to maximize liquid fuel production. The generations and individuals were 1000 and 1000, respectively [7]. The probabilities of the mutation and the crossover of individuals' genes were 0.005 and 0.005, respectively.

2.3.3. Fourier-transform infrared spectroscopy (FTIR)

FTIR test was conducted to determine the liquid fuel's main functional groups. The FTIR spectra were recorded from 4000 to 400 cm^{-1} with 4 cm^{-1} resolution by the Thermo Nicolet 6700 FTIR optical spectrometer.

2.3.4. Gas chromatography-mass spectrometry (GC-MS)

The specific components of the liquid fuel were determined by gas chromatography-mass spectrometry (GC-MS). The experiments were conducted by using a low-resolution Thermo Scientific TRACE 1300/1310 gas chromatograph coupled to a TSQ 9000 triple quadrupole mass spectrometer from Thermo Fisher (USA).

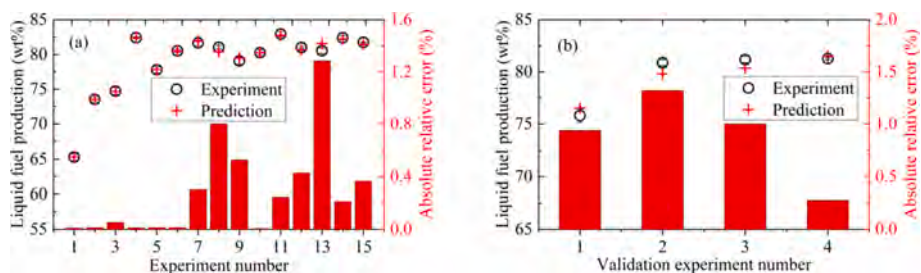


Fig. 3. The experimental and the adaptive neural fuzzy model predicted liquid fuel productions: (a) Training; (b) Testing.

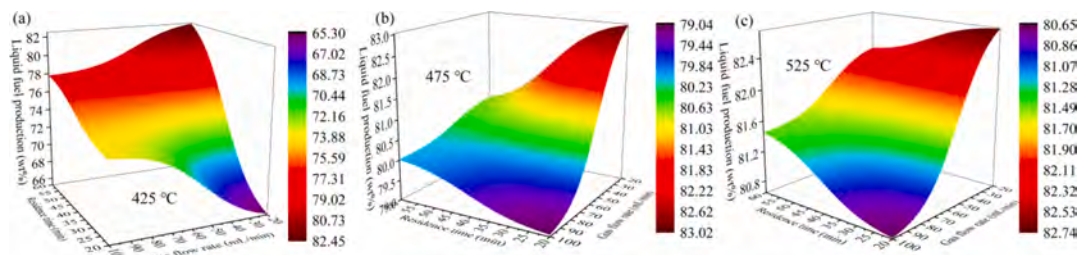


Fig. 4. Interactive effects of residence time and carrier gas flow rate on liquid fuel production at different temperatures: (a) 425 °C; (b) 475 °C; (c) 525 °C.

The temperatures of the GC front inlet and the MS transfer line were set at 280 °C. The GC front inlet was operated in the split mode. Helium was used as the carrier gas with a 1 mL/min flow rate. A polar phase ZB-5MS capillary column (30 m × 0.25 mm, ID × 0.25 μm film) was utilized. The GC oven was set to hold at 70 °C for 2 min, then increased to 250 °C with a heating rate of 10 °C/min and hold for 10 min, and lastly, increased to 300 °C with a heating rate of 20 °C/min and hold for 27.5 min. The MS was performed under the following conditions: ion source temperature, 230 °C; full scan, 30 Da-800 Da. The components were identified by the National Institute of Standards and Technology (NIST) mass spectrum library.

3. Results and discussion

3.1. Liquid fuel production

3.1.1. Accuracy of the adaptive neural fuzzy model

Fig. 3 illustrates the experimental and the adaptive neural fuzzy model predicted liquid fuel productions under different operating conditions. It is worth noting that liquid fuel's appearance resembles wax at room temperature [21,22].

Fig. 3a shows that the adaptive neural fuzzy model predicted liquid fuel production results were close to the experimental ones (E1-E15). The absolute relative errors between the predicted and the experimental values were within 1.3%. Moreover, the R-squared value between the experimental and the adaptive neural fuzzy model predicted liquid fuel productions was 0.9934. Fig. 3b exhibits the adaptive neural fuzzy model's applicability through the four additional experiments (V1-V4). The absolute relative errors between the predicted and the experimental values were within 1.4%. It reveals that the adaptive neural fuzzy model

predicted liquid fuel production is accurate and reliable.

3.1.2. Interactive effects of residence time and carrier gas flow rate on liquid fuel production

Fig. 4a–c demonstrate the interactive effects of the residence time and the carrier gas flow rate on liquid fuel production at temperatures of 425 °C, 475 °C, and 525 °C, respectively. The liquid fuel production varied from 65.32 wt% to 82.43 wt% at 425 °C; from 79.05 wt% to 83.00 wt% at 475 °C; and from 80.65 wt% to 82.73 wt% at 525 °C, respectively. Das and Tiwari [32] obtained around 81.4 wt% liquid fuel through thermal pyrolysis of virgin PE under the operating conditions of 400 °C, 8 h and 200 mL/min in a 1000 mL semi-batch reactor. They also obtained around 82.7 wt% liquid fuel under the operating conditions of 500 °C, 30 min, and 100 mL/min in the same reactor [8]. Onwudili et al. [3] obtained 89.5 wt% liquid fuel production at 425 °C in a batch reactor. However, Quesada et al. [21] obtained relatively lower liquid fuel production through the pyrolysis of WPE at 450 °C, which varied from 13.61 wt% to 48.38 wt%. This is because that they conducted the experiments under higher heating rates (20–50 °C/min).

As depicted in Fig. 4a, a higher carrier gas flow rate could increase liquid fuel production under a shorter residence time at 425 °C. For instance, the liquid fuel production was increased from 65.32 wt% to 73.54 wt% when the carrier gas flow rate varied from 20 mL/min to 100 mL/min under residence time of 20 min. Muhammad et al. [24] investigated liquid fuel production by the thermal pyrolysis of linear low-density PE at 450–460 °C. The liquid fuel production increased from 45.0 wt% to 75.0 wt% when the carrier gas flow rate varied from 0 to 60 mL/min. This is consistent with the results of this study. The increase in liquid fuel production could be attributed to the higher carrier gas flow rate, which can quickly carry volatile products out of the reactor,

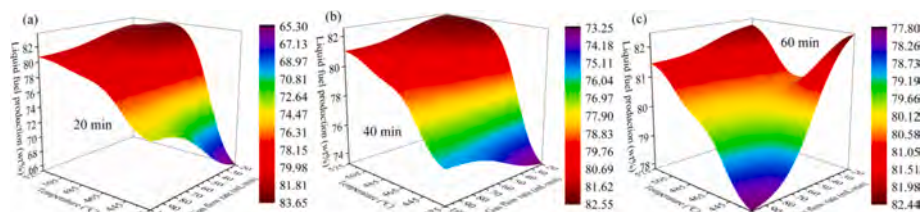


Fig. 5. Interactive effects of temperature and carrier gas flow rate on liquid fuel production under different residence times: (a) 20 min; (b) 40 min; (c) 60 min.

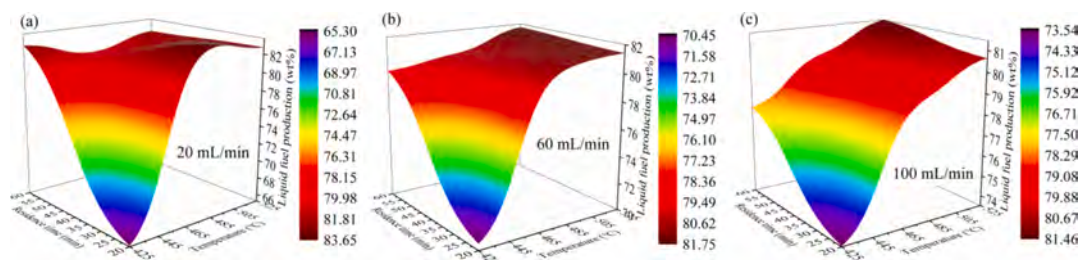


Fig. 6. Interactive effects of temperature and residence time on liquid fuel production under different carrier gas flow rates: (a) 20 mL/min; (b) 60 mL/min; (c) 100 mL/min.

thereby inhibiting the secondary reactions that consume liquid fuel [37]. However, the liquid fuel production was decreased with the increasing carrier gas flow rate under a longer residence time at 425 °C. For example, the liquid fuel production was decreased from 82.43 wt% to 77.81 wt% when the carrier gas flow rate increased from 20 mL/min to 100 mL/min under residence time of 60 min. The reduction of liquid fuel production could be attributed to that the higher carrier gas flow rate inhibited polycondensation and repolymerization reactions of the pyrolysis gas for liquid fuel formation [38]. As for the liquid fuel production at higher temperatures, as shown in Fig. 4b and c, increasing the carrier gas flow rate would inhibit the liquid fuel production under the residence time ranging from 20 min to 60 min. This is because higher temperatures can promote the liquid fuel's secondary cracking to generate the shorter-chain pyrolysis gas [39].

3.1.3. Interactive effects of temperature and carrier gas flow rate on liquid fuel production

Fig. 5a-c show the interactive effects of the temperature and the carrier gas flow rate on liquid fuel production under residence times of 20 min, 40 min, and 60 min, respectively. The liquid fuel production had the same variation tendency under a higher carrier gas flow rate regardless of the residence time changes. The liquid fuel productions were increased when the temperature increased from 425 °C to 525 °C for all residence times. The liquid fuel production was increased from 73.54 wt% to 80.65 wt% (20 min), from 75.53 wt% to 81.02 wt% (40 min), and from 77.81 wt% to 81.45 wt% (60 min) when temperature increased from 425 °C to 525 °C, respectively. The increase in the liquid fuel production could be attributed to more intense random scission reactions of WPE at higher temperatures [11]. The temperature has a more complex influence on liquid fuel production under the lowest carrier gas flow rate (20 mL/min). This is due to the interaction between the random scission reactions of WPE and the liquid fuel's secondary cracking reactions [37]. As illustrated in Fig. 5a, the liquid fuel production was firstly increased from 65.32 wt% to 83.63 wt% when temperature increased from 425 °C to 488 °C under residence time of 20 min. The increase in temperature had a greater impact on promoting random scission reactions of WPE in this temperature range. Therefore, the liquid fuel production increased with the increasing temperature. However, liquid fuel's secondary cracking reactions hold a dominant position in the higher temperature range. The liquid fuel production was

then decreased from 83.63 wt% to 82.73 wt% when temperature increased from 488 °C to 525 °C under residence time of 20 min. While the changing trend of liquid fuel production under residence time of 60 min, as shown in Fig. 5c, was a reversal from the one under residence time of 20 min. It indicated that the dominance of the random scission reactions of WPE and the secondary cracking reactions of the liquid fuel had been reversed under the longest residence time (60 min).

3.1.4. Interactive effects of temperature and residence time on liquid fuel production

Fig. 6a-c display the interactive effects of the temperature and the residence time on liquid fuel production under carrier gas flow rates of 20 mL/min, 60 mL/min, and 100 mL/min, respectively. The temperature has a more significant impact on liquid fuel production when the residence time is shorter under all carries gas flow rates. The residence time has less impact at higher temperatures [21]. As depicted in Fig. 6c, the liquid fuel production was increased with the increasing residence time regardless of the temperature. WPE could be fully decomposed into short-chain hydrocarbons with longer residence time through random scission reactions in the reactor [23]. Therefore, compared with the shorter residence time, the liquid fuel production was higher under longer residence time. The thermochemical conversion is an endothermic reaction, thereby increasing temperature is conducive to the thermal pyrolysis of WPE [40]. Thus, a higher temperature could improve liquid fuel production. It is noteworthy that liquid fuel production was decreased with the temperature above 500 °C under carries gas flow rate of 20 mL/min in the lower range of the residence time. Sharuddin et al. [6] also suggested that temperatures below 500 °C are more conducive to liquid fuel production. It could be attributed to that the liquid fuel was further decomposed into low-molecular pyrolysis gas through β cleavage reactions at temperatures over 500 °C [41,42].

3.2. Gas production

3.2.1. Accuracy of the adaptive neural fuzzy model

Fig. 7 depicts the experimental and the adaptive neural fuzzy model predicted gas production results under different operating conditions. As illustrated in Fig. 7a, the gas productions predicted by the adaptive neural fuzzy model were all close to the experimental ones (E1-E15). The absolute relative errors between the predicted and the experimental

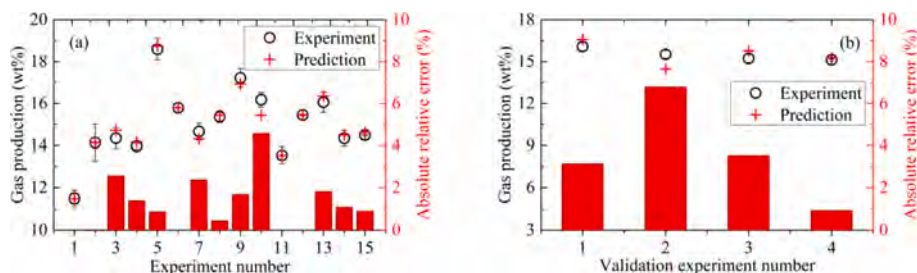


Fig. 7. The comparisons of the experimental and the adaptive neural fuzzy model predicted gas productions: (a) Training; (b) Testing.

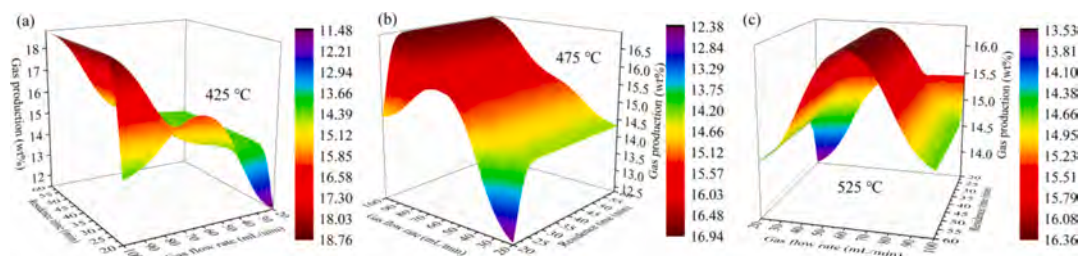


Fig. 8. Interactive effects of residence time and carrier gas flow rate on gas production at different temperatures: (a) 425 °C; (b) 475 °C; (c) 525 °C.

values were within 4.6%. Besides, the R-squared value between the experimental and the adaptive neural fuzzy model predicted gas production was 0.9719. The predicted gas production was relatively less accurate than the predicted liquid fuel production. This is because the gas production was calculated from the difference between the initial WPE mass and the masses of liquid fuel and residue. Errors in gas production were accumulated, and thereby gas production became more inaccurate [21]. Fig. 7b shows the applicability of the adaptive neural fuzzy model predicted gas production. The absolute relative errors between the predicted and the experimental values were within 6.8%. Quesada et al. [21] adopted the fuzzy neural model to predict the WPE thermal pyrolysis's energy efficiency. The maximum absolute relative error was approximately 6.4%. The errors of the predicted gas production were in a reasonable range in this study. Therefore, the adaptive neural fuzzy model is qualified to predict gas production.

3.2.2. Interactive effects of residence time and carrier gas flow rate on gas production

Fig. 8a–c illustrate the interactive effects of the residence time and the carrier gas flow rate on gas production at temperatures of 425 °C, 475 °C, and 525 °C, respectively. The gas production varied from 11.50 wt% to 18.75 wt% at 425 °C; from 12.40 wt% to 16.93 wt% at 475 °C; and from 13.54 wt% to 16.35 wt% at 525 °C, respectively. Onwudili et al. [3] obtained 10 wt% and 25 wt% gas productions through thermal pyrolysis of low-density PE in a batch reactor at temperatures of 425 °C and 450 °C, respectively. These results were similar to the ones reported by [8,32]. Gas productions of 16.58–22.53 wt% and 17.80–27.52 wt% were obtained through thermal pyrolysis of virgin low-density PE and high-density PE within the temperature ranging from 350 °C to 400 °C, respectively [32]. Also, approximately 17 wt% of gas was obtained at a temperature of 500 °C [8].

As demonstrated in Fig. 8a, a longer residence time would increase the gas production under the lowest (20 mL/min) and the highest (100 mL/min) carrier gas flow rates at 425 °C. When the residence time was increased from 20 min to 60 min, the gas production was increased from 11.50 to 14.17 wt% and 14.14–18.75 wt% under the carrier gas flow rates of 20 mL/min and 100 mL/min, respectively. Onwudili et al. [3] also found that gas production was increased from 8.70 wt% to 16.30 wt% at 450 °C when the residence time increased from 0 min to 30 min. This is because the random scission reactions of WPE were not intense to produce pyrolysis gas at low temperatures [37]. Extending the residence time could make the random scission reactions of WPE proceed more

thoroughly to obtain higher gas yields. As shown in Fig. 8b, the carrier gas flow rate had a stronger impact on gas production under the lowest residence time (20 min) at 475 °C. The gas production was first increased from 12.40 wt% to 15.82 wt% when the carrier gas flow rate increased from 20 mL/min to 64 mL/min. The increase in gas production could be attributed to the inhibition of polycondensation and repolymerization reactions of the pyrolysis gas at low carrier gas flow rates [38]. While the excessive carrier gas flow rate would reduce the heat transfer efficiency inside the reactor, thereby inhibiting the gas production [37]. Thus, gas production decreased from 15.82 wt% to 14.72 wt% when the carrier gas flow rate varied from 64 mL/min to 100 mL/min. The thermal pyrolysis of linear low-density PE at 450–460 °C has a similar phenomenon [24]. The gas production was first increased from 15.5 wt% to 20.0 wt% (by difference) when the carrier gas flow rate increased from 0 mL/min to 30 mL/min. Then, the gas production decreased from 20.0 wt% to 17.5 wt% when the carrier gas flow rate varied from 30 mL/min to 60 mL/min. At 525 °C, as depicted in Fig. 8c, a longer residence time would increase gas production under the lowest carrier gas flow rate (20 mL/min). The gas production was increased from 13.54 wt% to 14.49 wt% when the residence time increased from 20 min to 60 min. This is because that longer residence time enhanced the possibility of β cleavage reactions for pyrolysis gas formation [41].

3.2.3. Interactive effects of temperature and carrier gas flow rate on gas production

Fig. 9a–c present the interactive effects of the temperature and the carrier gas flow rate on gas production under residence times of 20 min, 40 min, and 60 min, respectively. The carrier gas flow rate had a stronger influence on gas production at the lowest temperature (425 °C) regardless of residence time changes. As illustrated in Fig. 9a, the temperature had a similar influence on gas production under the lowest (20 mL/min) and the highest (100 mL/min) carrier gas flow rates. The gas productions were both increased with the increasing temperature. The liquid fuel's secondary cracking reactions were more intense to generate pyrolysis gas at higher temperatures [37]. However, the temperature had an opposite impact on the gas production under the medium (60 mL/min) carrier gas flow rate. The gas production was decreased from 16.17 wt% to 15.30 wt% when the temperature increased from 425 °C to 525 °C. The gas production was also decreased from 55.46 wt% to 32.63 wt% when the temperature varied from 450 °C to 550 °C in [21]. The increase in temperature promoted polycondensation and repolymerization reactions of the pyrolysis gas, resulting in a reduction in gas

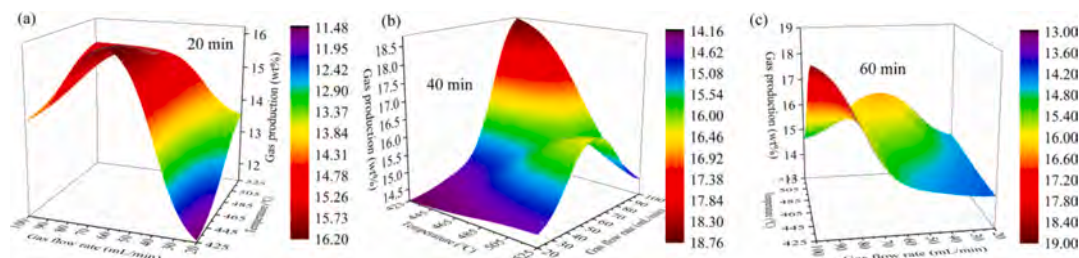


Fig. 9. Interactive effects of temperature and carrier gas flow rate on gas production under different residence times: (a) 20 min; (b) 40 min; (c) 60 min.

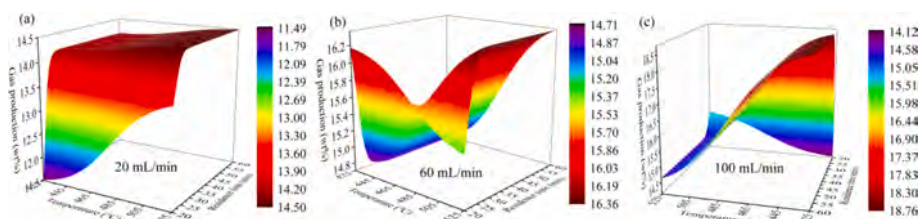


Fig. 10. Interactive effects of temperature and residence time on gas production under different carrier gas flow rates: (a) 20 mL/min; (b) 60 mL/min; (c) 100 mL/min.

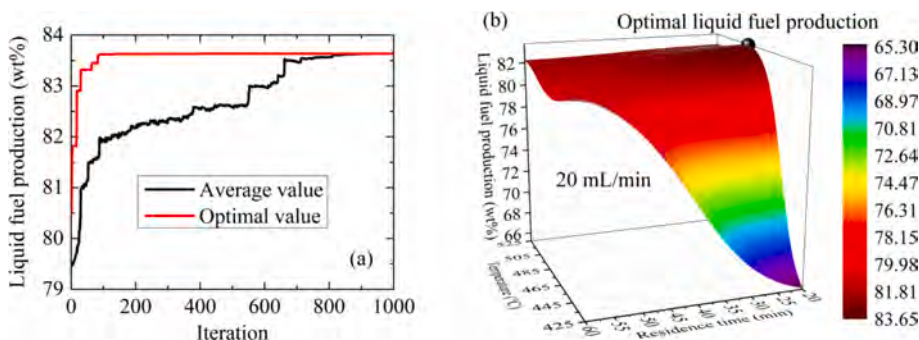


Fig. 11. Illustrations of optimized operating conditions by GA: (a) Optimization process; (b) Liquid fuel production under optimal operating conditions.

production. It also suggested that the polycondensation and repolymerization reactions of the pyrolysis gas played a dominant role, compared to the secondary cracking reactions of the liquid fuel, under the medium carrier gas flow rate (60 mL/min). As depicted in Fig. 9b and c, the temperature and the carrier gas flow rate had the same influences on gas production under the residence times of 40 min and 60 min. The lowest gas productions were obtained under the same operating conditions (temperature of 425 °C and carrier gas flow rate of 20 mL/min). While the highest gas productions were both obtained under 425 °C and 100 mL/min. It indicated that a higher carrier gas flow rate could suppress the polycondensation and repolymerization reactions for the pyrolysis gas consumption under the residence times of 40 min and 60 min.

3.2.4. Interactive effects of temperature and residence time on gas production

Fig. 10a–c demonstrate the interactive effects of the temperature and the residence time on gas production under carrier gas flow rates of 20

mL/min, 60 mL/min, and 100 mL/min, respectively. As shown in Fig. 10a, the temperature could enhance gas production under the carrier gas flow rate of 20 mL/min regardless of the residence time changes. As depicted in Fig. 10b and c, the interactive effects of the temperature and the residence time became more complicated on gas production under the carrier gas flow rates of 60 mL/min and 100 mL/min. For example, as demonstrated in Fig. 10b, the gas production was decreased from 16.17 wt% to 14.71 wt% when the residence time increased from 20 min to 60 min at 425 °C and 60 mL/min. The reason for the decrease in gas production was the promotion of the pyrolysis gas polymerization reactions at a longer residence time. Concurrently, the gas production was increased from 15.30 wt% to 16.35 wt% when the residence time varied from 20 min to 60 min at 525 °C and 60 mL/min. The longer residence time enhanced the possibility of char gasification and β cleavage reactions for pyrolysis gas formation [37]. As depicted in Fig. 10c, the residence time's influence on gas production was opposite under 100 mL/min, compared with the results under 60 mL/min. Longer residence time would enhance the gas production at 425 °C; while it would inhibit the gas production at 525 °C.

3.3. Optimization of operating conditions by GA

As discussed in Section 3.1, the operating conditions (temperature, residence time, and carrier gas flow rate) had very complex interactive effects on liquid fuel production. To obtain the maximum liquid fuel production, GA was adopted to determine the optimal operating conditions. Fig. 11a exhibits the variations of the average and the optimal values of 1000 individuals' fitness in 1000 iterations. In this study, fitness was liquid fuel production. The optimal value reached stability after 100 iterations, while the average value was stabilized after 800 iterations.

Fig. 11b shows the maximum liquid fuel production under the optimal operating conditions. The GA optimized operating conditions were 488 °C, 20 min, and 20 mL/min. The optimal liquid fuel production was 83.63 wt%. Rodríguez-Luna et al. [23] reported 500 °C was the most suitable temperature for pyrolysis of high-density PE to produce liquid fuel in a semi-batch reactor. Quesada et al. [21] concluded that the optimal operating conditions for liquid fuel production were 500 °C and 120 min. The experiments were conducted in a horizontal tubular

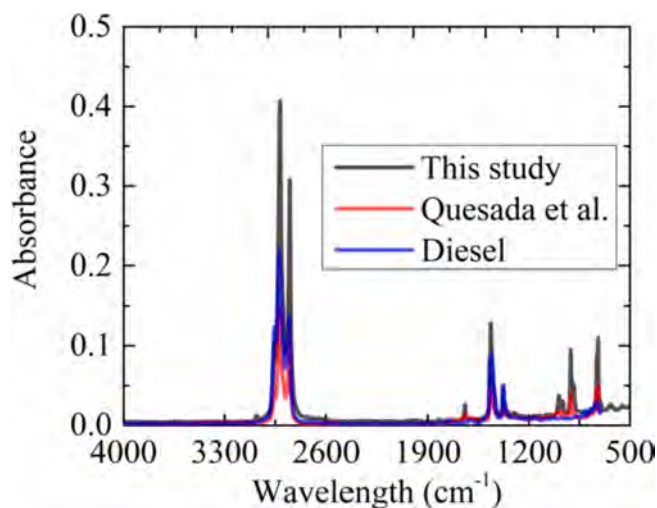


Fig. 12. FTIR analysis of liquid fuels from this study and Quesada et al. [22], and diesel [22].

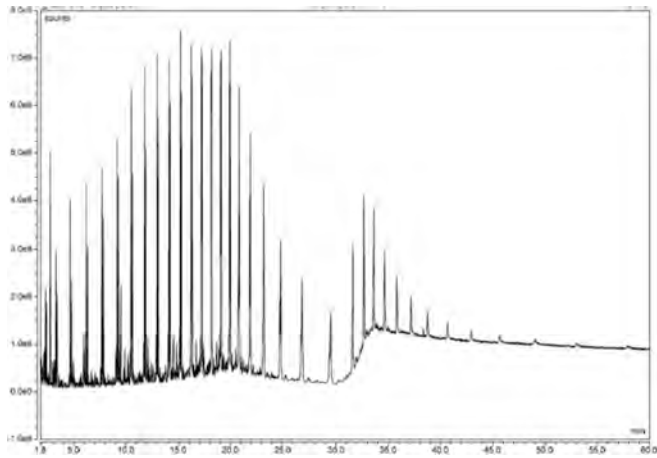


Fig. 13. GC-MS analysis of the liquid fuel under the optimal operating conditions (488 °C, 20 min, and 20 mL/min).

reactor. The optimized temperature was close to the one in this study. While the optimized residence time was much longer than the one in this study. This is because the experiments in [21] were conducted under higher heating rates (20–50 °C/min) and a faster carrier gas flow rate (833 mL/min). Sharuddin et al. [6] also concluded that temperatures below 500 °C were suitable for liquid fuel production.

The experiment under GA optimized operating conditions (488 °C, 20 min, and 20 mL/min) was conducted to verify the GA predicted results. The experimental liquid fuel production was 83.50 ± 0.59 wt%. The absolute relative error between the predicted and the experimental values was within 0.16%. It suggests that the GA optimized results were accurate and reliable.

3.4. FTIR analysis

Fig. 12 shows the FTIR results of liquid fuels from this study and Quesada et al. [22]. The main functional groups of liquid fuels do not change under different operating conditions [22]. Therefore, the liquid fuel under the optimal operating conditions (488 °C, 20 min, and 20 mL/min) was chosen to conduct the FTIR analysis. As illustrated in Fig. 12, the following functional groups in liquid fuel of this study were determined: C–H stretch at $2916\text{--}2848\text{ cm}^{-1}$ [43]; C–C stretching at 1642 cm^{-1} and 1462 cm^{-1} ; C–H scissor and bend at 1377 cm^{-1} ; C–H out of the plane bend at 909 cm^{-1} ; and C–H bend at 719 cm^{-1} . The linear alkanes were generated by intermolecular hydrogen transfer reactions [44]. While the β cleavage coupled with the intramolecular hydrogen transfer reactions are responsible for the alkenes yields during the pyrolysis of WPE [23].

Fig. 12 also demonstrates the FTIR results of liquid fuel from Quesada et al. [22] and diesel. The liquid fuel sample in [22] was obtained under 500 °C, 80 min, and 833 mL/min. The liquid fuel from this study had the same characteristic peaks like the one in [22]. It also suggests that the operating conditions do not change the main functional groups of WPE thermal pyrolysis liquid fuels. Besides, the liquid fuel from this study had similar characteristic peaks as diesel.

3.5. GC-MS analysis

The GC-MS analysis was conducted to determine the specific components of the liquid fuel. Fig. 13 demonstrates the liquid fuel chromatogram under the optimal operating conditions (488 °C, 20 min, and 20 mL/min). The identified compounds present in the liquid fuel under the optimal operating conditions are tabulated in Table 2. The components of the liquid fuel were mainly 1-alkenes and n-alkanes ranging from C7 to C36. The liquid fuel's mean molecular weight was 291 g/mol.

Fig. A.1-15 illustrate the chromatograms of the liquid fuels E1-15,

Table 2

Identified compounds present in the liquid fuel under the optimal operating conditions (488 °C, 20 min, and 20 mL/min).

Peak	Time (min)	Compound	Relative area (%)	Molecular weight
1	2.32	cyclopentane (C7)	0.71	98
2	2.38	n-heptane (C7)	0.63	100
3	2.76	1-octene (C8)	1.67	112
4	2.98	n-octane (C8)	0.20	114
5	3.31	1-nonene (C9)	1.41	126
6	3.40	n-nonane (C9)	0.74	128
7	4.66	1-decene (C10)	1.33	140
8	4.79	n-decane (C10)	0.78	142
9	6.19	1-undecene (C11)	1.51	154
10	6.31	n-undecane (C11)	1.01	156
11	7.70	1-dodecene (C12)	1.53	168
12	7.82	n-dodecane (C12)	1.21	170
13	9.15	1-tridecene (C13)	1.75	182
14	9.26	n-tridecane (C13)	2.12	184
15	10.50	1-tetradecene (C14)	2.09	196
16	10.60	n-tetradecane (C14)	1.47	198
17	11.78	1-pentadecene (C15)	2.18	210
18	11.87	n-pentadecane (C15)	1.66	212
19	12.99	1-hexadecene (C16)	2.45	224
20	13.07	n-hexadecane (C16)	2.01	226
21	14.13	1-heptadecene (C17)	2.62	238
22	14.20	n-heptadecane (C17)	2.08	240
23	15.21	1-octadecene (C18)	2.87	252
24	15.28	n-octadecane (C18)	2.39	254
25	16.24	1-nonadecene (C19)	2.74	266
26	16.30	n-nonadecane (C19)	2.35	268
27	17.21	1-eicosene (C20)	2.54	280
28	17.27	n-eicosane (C20)	2.50	282
29	18.15	1-heneicosene (C21)	2.66	294
30	18.20	n-heneicosane (C21)	2.64	296
31	19.04	1-docosene (C22)	2.62	308
32	19.09	n-docosane (C22)	2.89	310
33	19.90	1-tricosene (C23)	2.24	322
34	19.94	n-tricosane (C23)	2.63	324
35	20.79	1-tetracosene (C24)	2.10	336
36	20.83	n-tetracosane (C24)	2.75	338
37	21.83	1-pentacosene (C25)	1.93	350
38	21.88	n-pentacosane (C25)	2.76	352
39	23.11	1-hexacosene (C26)	1.66	364
40	23.17	n-hexacosane (C26)	2.71	366
41	24.71	1-heptacosene (C27)	1.22	378
42	24.79	n-heptacosane (C27)	2.59	380
43	26.75	1-octacosene (C28)	1.31	392
44	26.84	n-octacosane (C28)	2.60	394
45	29.36	1-nonacosene (C29)	0.88	406
46	29.47	n-nonacosane (C29)	2.37	408
47	31.56	1-triacontene (C30)	0.82	420
48	31.60	n-triacontane (C30)	2.27	422
49	33.60	n-hentriacontane (C31)	2.18	436
50	34.64	n-dotriacontane (C32)	1.80	450
51	35.81	n-tritriacontane (C33)	1.54	464
52	37.16	n-tetracontane (C34)	1.00	478
53	38.76	n-pentatriacontane (C35)	0.72	492
54	40.67	n-hexatriacontane (C36)	0.58	506

respectively. The liquid fuels E1-15 had the same component types as the liquid fuel under the optimal operating conditions (mostly 1-alkenes and n-alkanes ranging from C7 to C36). However, the specific component proportions of the liquid fuels were different. This indicated that the operating conditions had effects on the composition of the liquid fuel produced by the thermal pyrolysis of waste polyethylene. The liquid fuel was classified into light (C7 – C11), middle (C12 – C20) and heavy (C21 – C36) fractions [8]. Fig. 14 shows the liquid fuel fractions and mean molecular weight under different operating conditions. The light, middle and heavy fractions varied from 3.61 to 6.79%, 28.65–42.54% and 50.72–66.83%, respectively. Moreover, the liquid fuel's mean molecular weight was varied from 291.00 g/mol to 325.23 g/mol.

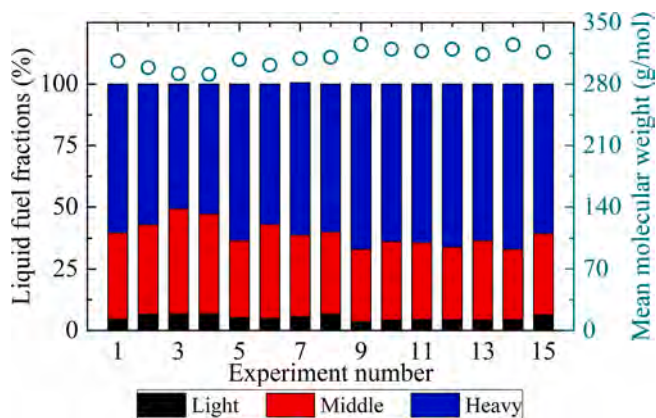


Fig. 14. Liquid fuel fractions and mean molecular weight under different operating conditions.

Fig. 15 demonstrates the effects of operating conditions on liquid fuel fractions and mean molecular weight. Samples of E3, E8 and E13 were taken into consideration to analyze the effect of temperature on the liquid fuel composition. As shown in Fig. 15a, the light and middle fractions were decreased from 6.74 to 4.25% and 42.54–32.22% when the temperature was increased from 425 °C to 525 °C, respectively. In comparison, the heavy fraction was increased from 50.72% to 63.53% when the temperature was increased from 425 °C to 525 °C. Besides, the liquid fuel's mean molecular weight was also increased from 291.78 g/mol to 313.96 g/mol. This indicates that high temperature is conducive to the formation of the heavy fraction in the liquid fuel. It can be ascribed to that higher temperature would enhance the possibility of secondary reactions of liquid fuel's light and middle fractions for pyrolysis gas formation [8].

Fig. 15b illustrates the effect of residence time on liquid fuel fractions and mean molecular weight (E6, E8 and E10). The middle fraction was decreased from 38.18% to 32.02%, whereas the heavy fraction was increased from 56.80% to 63.73% when residence time was increased from 20 min to 60 min. The light fraction was firstly increased from

5.02% to 6.73% when residence time was increased from 20 min to 40 min. The light fraction was then decreased from 6.73% to 4.25% when residence time varied from 40 min to 60 min. The longer residence time enhanced the possibility of β cleavage reactions of liquid fuel's light and middle fractions [8,37]. Therefore, the liquid fuel's mean molecular weight was increased from 301.54 g/mol to 319.73 g/mol when residence time was increased from 20 min to 60 min.

Fig. 15c shows the effect of carrier gas flow rate on liquid fuel fractions and mean molecular weight (E7, E8 and E9). The light, middle and heavy fractions varied from 3.61 to 6.73%, 29.57–33.42% and 59.86–66.82%, respectively. Moreover, the liquid fuel's mean molecular weight was increased from 309.02 g/mol to 325.23 g/mol when the carrier gas flow rate increased from 20 mL/min to 100 mL/min. The increase in liquid fuel's mean molecular weight could be attributed to the higher carrier gas flow rate, which can quickly carry volatile products out of the reactor, thereby inhibiting β cleavage reactions of liquid fuel's heavy fraction [37] and polycondensation and repolymerization reactions of the pyrolysis gas [38] for the light and middle fractions' liquid fuel formation.

4. Conclusion

This study aims to obtain the optimal operating conditions for liquid fuel production through thermal pyrolysis of waste polyethylene in a bench-scale semi-batch reactor. Three operating conditions were considered, i.e., the temperature, the residence time, and the carrier gas flow rate. The adaptive neural fuzzy model comprehensively described the interactive effects of operating conditions on liquid fuel production. The R-squared value between the experimental and the adaptive neural fuzzy model predicted liquid fuel production was 0.9934. It revealed that the adaptive neural fuzzy model predicted liquid fuel production was accurate and reliable.

Subsequently, the genetic algorithm (GA) was adopted to optimize the operating conditions to maximize liquid fuel production. The GA optimized liquid fuel production was 83.63 wt% under the operating conditions of 488 °C (temperature), 20 min (residence time) and 20 mL/min (carrier gas flow rate). The experimental liquid fuel production was 83.50 wt% under these operating conditions, a value very close to the

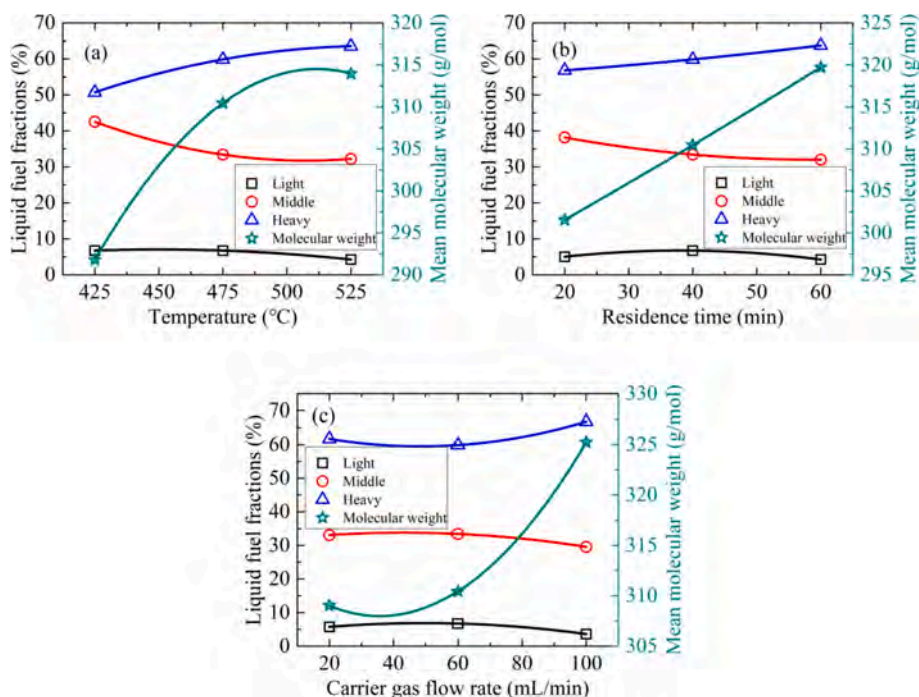


Fig. 15. Effects of operating conditions on liquid fuel fractions and mean molecular weight: (a) Temperature; (b) Residence time; (c) Carrier gas flow rate.

GA predicted one. It indicated that the adaptive neural fuzzy model coupled with GA was qualified to optimize the operating conditions for liquid fuel production through thermal pyrolysis of waste polyethylene.

FTIR and GC-MS analyses were conducted to determine the liquid fuels' main functional groups and the chemical components. It was found that the operating conditions did not change the liquid fuels' main functional groups. The waste polyethylene thermal pyrolysis liquid fuels had similar characteristic peaks as commercial diesel. The liquid fuels had the same component types under different operating conditions (mostly 1-alkenes and n-alkanes ranging from C7 to C36). However, the specific component proportions of the liquid fuels varied with the operating conditions. It could be concluded that high temperature, long residence time and high carrier gas flow rate were conducive to formation of the liquid fuel's heavy fraction. While low temperature, short residence time and low carrier gas flow rate were beneficial to form light and middle fractions in liquid fuel.

Declaration of Competing Interest

The authors declare that they have no known competing financial interests or personal relationships that could have appeared to influence the work reported in this paper.

Acknowledgements

This work was supported by the China Scholarship Council (CSC) program (No. 201906120036). Thanks are given to Dr. Yue ZAN from LCC-CNRS-UPS (Laboratoire de Chimie de Coordination du CNRS, Université Toulouse III - Paul Sabatier) for her assistance in the FTIR test and analysis.

Appendix A. Supplementary data

Supplementary data to this article can be found online at <https://doi.org/10.1016/j.enconman.2021.114114>.

References

- [1] Kaza, S.; Yao, L. C.; Bhada-Tata, P.; Van Woerden, F. What a Waste 2.0: A Global Snapshot of Solid Waste Management to 2050. 2018. <http://datatopics.worldbank.org/what-a-waste/>.
- [2] Quesada L, Calero M, Martin-Lara MA, Perez A, Blazquez G. Production of an alternative fuel by pyrolysis of plastic wastes mixtures. *Energ Fuel* 2020;34:1781–90. <https://doi.org/10.1021/acs.energyfuels.9b03350>.
- [3] Onwudili JA, Insura N, Williams PT. Composition of products from the pyrolysis of polyethylene and polystyrene in a closed batch reactor: Effects of temperature and residence time. *J Anal Appl Pyrolysis* 2009;86:293–303. <https://doi.org/10.1016/j.jaap.2009.07.008>.
- [4] Geyer R, Jambeck JR, Law KL. Production, use and fate of all plastics ever made. *Sci Adv* 2017;3(7):1–5. <https://doi.org/10.1126/sciadv.1700782>.
- [5] Crippa, M.; De Wilde, B.; Koopmans, R.; Leyssens, J.; Muncke, J.; Ritschkoff A-C.; Van Doorselaer, K.; Velis, C.; Wagner, M. A circular economy for plastics - Insights from research and innovation to inform policy and funding decisions, 2019 (M. De Smet & M. Linder, Eds.). European Commission, Brussels, Belgium. <https://doi.org/10.2777/269031>.
- [6] Sharuddin SDA, Abnisa F, Daud WMAW, Aroua MK. A review on pyrolysis of plastic wastes. *Energy Convers Manag* 2016;115:308–26. <https://doi.org/10.1016/j.enconman.2016.02.037>.
- [7] Pan R, Duque JVF, Debenest G. Investigating waste plastic pyrolysis kinetic parameters by genetic algorithm coupled with thermogravimetric analysis. *Waste Biomass Valori* 2020. <https://doi.org/10.1007/s12649-020-01181-4>.
- [8] Das P, Tiwari P. The effect of slow pyrolysis on the conversion of packaging waste plastics (PE and PP) into fuel. *Waste Manage* 2018;79:615–24. <https://doi.org/10.1016/j.wasman.2018.08.021>.
- [9] Ceamanos J, Mastral JF, Millera A, Aldea ME. Kinetics of pyrolysis of high density polyethylene. Comparison of isothermal and dynamic experiments. *J Anal Appl Pyrolysis* 2002;65(2):93–110. [https://doi.org/10.1016/S0165-2370\(01\)00183-8](https://doi.org/10.1016/S0165-2370(01)00183-8).
- [10] Mazloum S, Awad S, Allam N, Aboussallem Y, Loubar K. Modelling plastic heating and melting in a semi-batch pyrolysis reactor. *Appl Energy* 2021;283:116375. <https://doi.org/10.1016/j.apenergy.2020.116375>.
- [11] Al-Salem SM, Antelava A, Constantinou A, Manos G, Dutta A. A review on thermal and catalytic pyrolysis of plastic solid waste (PSW). *J Environ Manage* 2017;197:177–98. <https://doi.org/10.1016/j.jenvman.2017.03.084>.
- [12] Kunwar B, Cheng HN, Chandrashekar SR, Sharma BK. Plastics to fuel: a review. *Renew Sust Energ Rev* 2016;54:421–8. <https://doi.org/10.1016/j.rser.2015.10.015>.
- [13] Manos G, Garforth A, Dwyer J. Catalytic degradation of high-density polyethylene on an ultrastable-Y Zeolite. Nature of initial polymer reactions, pattern of formation of gas and liquid products, and temperature effects. *Ind Eng Chem Res* 2000;39(5):1203–8. <https://doi.org/10.1021/ie990513i>.
- [14] Manos G, Yusof IY, Gangas NH, Papayannakos N. Tertiary recycling of polyethylene to hydrocarbon fuel by catalytic cracking over aluminum pillared clays. *Energ Fuel* 2002;16(2):485–9. <https://doi.org/10.1021/ef0102364>.
- [15] Quesada L, de Hoces MC, Martin-Lara MA, Luzon G, Blazquez G. Performance of different catalysts for the in situ cracking of the oil-waxes obtained by the pyrolysis of polyethylene film waste. *Sustainability* 2020;12(13):5482. <https://doi.org/10.3390/su12135482>.
- [16] Kassargy C, Awad S, Burnens G, Kahine K, Tazerout M. Experimental study of catalytic pyrolysis of polyethylene and polypropylene over USY zeolite and separation to gasoline and diesel-like fuels. *J Anal Appl Pyrolysis* 2017;127:31–7. <https://doi.org/10.1016/j.jaap.2017.09.005>.
- [17] Al-Salem SM. Thermal pyrolysis of high density polyethylene (HDPE) in a novel fixed bed reactor system for the production of high value gasoline range hydrocarbons (HC). *Process Saf Environ* 2019;127(B):171–9. <https://doi.org/10.1016/j.psep.2019.05.008>.
- [18] Yan GX, Jing XD, Wen H, Xiang SG. Thermal cracking of virgin and waste plastics of PP and LDPE in a semibatch reactor under atmospheric pressure. *Energ Fuel* 2015;29(4):2289–98. <https://doi.org/10.1021/ef502919f>.
- [19] Insura N, Onwudili JA, Williams PT. Catalytic pyrolysis of low-density polyethylene over alumina-supported noble metal catalysts. *Energ Fuel* 2010;24(8):4231–40. <https://doi.org/10.1021/ef100227f>.
- [20] Tiikma L, Tamvelius H, Luik L. Coprocessing of heavy shale oil with polyethylene waste. *J Anal Appl Pyrolysis* 2007;79(1–2):191–5. <https://doi.org/10.1016/j.jaap.2006.12.029>.
- [21] Quesada L, Perez A, Godoy V, Peula FJ, Calero M, Blazquez G. Optimization of the pyrolysis process of a plastic waste to obtain a liquid fuel using different mathematical models. *Energy Convers Manag* 2019;188:19–26. <https://doi.org/10.1016/j.enconman.2019.03.054>.
- [22] Quesada L, Calero M, Martin-Lara MA, Perez A, Blazquez G. Characterization of fuel produced by pyrolysis of plastic film obtained of municipal solid waste. *Energy* 2019;186:115874. <https://doi.org/10.1016/j.energy.2019.115874>.
- [23] Rodríguez-Luna L, Bustos-Martínez D, Valenzuela E. Two-step pyrolysis for waste HDPE valorization. *Process Saf Environ Prot* 2021;149:526–36. <https://doi.org/10.1016/j.psep.2020.11.038>.
- [24] Muhammad I, Makwashi N, Manos G. Catalytic degradation of linear low-density polyethylene over HY-zeolite via pre-degradation method. *J Anal Appl Pyrolysis* 2019;138:10–21. <https://doi.org/10.1016/j.jaap.2018.11.025>.
- [25] Karaboga D, Kaya E. Adaptive network based fuzzy inference system (ANFIS) training approaches: A comprehensive survey. *Artif Intell Rev* 2019;52:2263–93. <https://doi.org/10.1007/s10462-017-9610-2>.
- [26] Jang JSR. ANFIS: adaptive-network-based fuzzy inference system. *IEEE T Syst Man Cy* 1993;23(3):665–85. <https://doi.org/10.1109/21.256541>.
- [27] Paramasivam B. Fuzzy prediction and RSM optimization of CI engine performance analysis: aegle marmelos non-edible seed cake pyrolysis oil as a diesel alternative. *Energ Source Part A* 2020. <https://doi.org/10.1080/15567036.2020.1773971>.
- [28] Pan RM, Duque JVF, Martins MF, Debenest G. Application of a neural fuzzy model combined with simulated annealing algorithm to predict optimal conditions for polyethylene waste non-isothermal pyrolysis. *Heliyon* 2020;6(11):e05598. <https://doi.org/10.1016/j.heliyon.2020.e05598>.
- [29] Al-Yaari M, Dubdub I. Application of artificial neural networks to predict the catalytic pyrolysis of HDPE using non-isothermal TGA data. *Polymers-Basel* 2020;12(8):1813. <https://doi.org/10.3390/polym12081813>.
- [30] Fakhrooseini SM, Dastanian M. Predicting pyrolysis products of PE, PP, and PET using NRTL activity coefficient model. *J Chem-NY* 2013, 2013;487676. <https://doi.org/10.1155/2013/487676>.
- [31] Ighose BO, Adeleke IA, Damos M, Junaid HA, Okpalaek KE, Betiku E. Optimization of biodiesel production from Thevetia peruviana seed oil by adaptive neuro-fuzzy inference system coupled with genetic algorithm and response surface methodology. *Energy Convers Manag* 2017;132:231–40. <https://doi.org/10.1016/j.enconman.2016.11.030>.
- [32] Das P, Tiwari P. Valorization of packaging plastic waste by slow pyrolysis. *Resour Conserv Recycl* 2018;128:69–77. <https://doi.org/10.1016/j.resconrec.2017.09.025>.
- [33] Lin YH, Yen HY. Fluidised bed pyrolysis of polypropylene over cracking catalysts for producing hydrocarbons. *Polym Degrad Stab* 2005;89(1):101–8. <https://doi.org/10.1016/j.polymdegradstab.2005.01.006>.
- [34] Lin YH, Yang MH. Catalytic pyrolysis of polyolefin waste into valuable hydrocarbons over reused catalyst from refinery FCC units. *Appl Catal A-Gen* 2007;328(2):132–9. <https://doi.org/10.1016/j.apcata.2007.05.039>.
- [35] Wang CX, Lei HW, Qian MRO, Huo EG, Zhao YF, Zhang QF, et al. Application of highly stable biochar catalysts for efficient pyrolysis of plastics: A readily accessible potential solution to a global waste crisis. *Sustain Energy Fuels* 2020;4:4614–24. <https://doi.org/10.1039/D0SE00652A>.
- [36] Lu XQ, Wu YB, Lian J, Zhang YY, Chen C, Wang PS, et al. Energy management of hybrid electric vehicles: A review of energy optimization of fuel cell hybrid power system based on genetic algorithm. *Energy Convers Manag* 2020;205:112474. <https://doi.org/10.1016/j.enconman.2020.112474>.
- [37] Xu FF, Ming X, Jia R, Zhao M, Wang B, Qiao YY, et al. Effects of operating parameters on products yield and volatiles composition during fast pyrolysis of

food waste in the presence of hydrogen 2020;210:106558. <https://doi.org/10.1016/j.fuproc.2020.106558>.

- [38] Heidari A, Stöhl R, Younesi H, Rashidi A, Troeger N, Ghoreyshi AA. Effect of process conditions on product yield and composition of fast pyrolysis of Eucalyptus grandis in fluidized bed reactor. *J Ind Eng Chem* 2014;20(4):2594-602. <https://doi.org/10.1016/j.jiec.2013.10.046>.
- [39] Wei F, Cao JP, Zhao XY, Ren J, Wang JX, Fan X, et al. Nitrogen evolution during fast pyrolysis of sewage sludge under inert and reductive atmospheres. *Energ Fuel* 2017;31(7):7191-6. <https://doi.org/10.1021/acs.energyfuels.7b00920>.
- [40] Morato-Godino A, Sánchez-Delgado S, García-Hernando N, Soria-Verdugo A. Pyrolysis of *Cynara cardunculus* L. samples – effect of operating conditions and bed stage on the evolution of the conversion. *Chem Eng J* 2018;351:371-81. <https://doi.org/10.1016/j.cej.2018.06.114>.
- [41] Cai N, Li XQ, Xia SW, Sun L, Hu JH, Bartocci P, et al. Pyrolysis-catalysis of different waste plastics over Fe/Al₂O₃ catalyst: High-value hydrogen, liquid fuels, carbon nanotubes and possible reaction mechanisms. *Energy Convers Manag* 2021;229:113794. <https://doi.org/10.1016/j.enconman.2020.113794>.
- [42] Vollmer I, Jenks MJF, Roelands MCP, White RJ, Harmelen T, Wild P, et al. Beyond mechanical recycling: Giving new life to plastic waste. *Angew Chem Int Ed* 2020; 59(36):15402-23. <https://doi.org/10.1002/anie.201915651>.
- [43] Ghenai C, Rasheed MA, Alshamsi MJ, Alkamali MA, Ahmad FF, Inayat A. Design of hybrid solar photovoltaics/shrouded wind turbine power system for thermal pyrolysis of plastic waste. *Case Stud Therm Eng* 2020;22:100773. <https://doi.org/10.1016/j.csite.2020.100773>.
- [44] McCaffrey WC, Cooper DG, Kamal MR. Tertiary recycling of polyethylene: mechanism of liquid production from polyethylene by thermolysis/reactive distillation. *Polym Degrad Stab* 1998;62(3):513-21. [https://doi.org/10.1016/S0141-3910\(98\)00036-6](https://doi.org/10.1016/S0141-3910(98)00036-6).